Experimental Demonstration of Dynamic Optical Beamforming for Beyond 5G Spatially Multiplexed Fronthaul Networks

Experimental Demonstration of Dynamic Optical Beamforming for Beyond 5G Spatially Multiplexed Fronthaul Networks

R. Muñoz, *Senior Member, IEEE,* S. Rommel, *Member, IEEE,* P. van Dijk, J. Brenes, E. Grivas, C. Manso, C. Roeloffzen, R. Vilalta, *Senior Member, IEEE,* J. M. Fabrega, *Senior Member, IEEE,* G. Landi, R. Casellas, *Senior Member, IEEE,* R. Martínez, *Senior Member, IEEE,* and I. Tafur Monroy *Senior Member, IEEE,*

(Invited Paper)

***Abstract*—This paper presents a beyond 5G fronthaul network with dynamic beamforming and -steering. The proposed fronthaul solution deploys optical beamforming (OBF) by combining space division multiplexing (SDM), analogue radio-over-fiber (ARoF), and the novel optical beam forming network (OBFN) technologies. From the service management and orchestration (MANO) point of view, the proposed fronthaul solution also deploys an advanced software defined networking (SDN) and Network Function Virtualization (NFV) control and orchestration architecture developed with the goal to optimally manage and reconfigure the physical layer resources (i.e., optical and radio) at the central office and cell sites (i.e., pool of baseband units (BBUs), remote radio heads (RRHs), ARoF transceivers and OBFNs). The proposed beyond 5G fronthaul architecture is primarily oriented to deploy massive machine-type communication (mMTC) services with high-bandwidth requirements, such as for industry 4.0. In this paper we experimentally validate the novel OBFN system, and the dynamic SDN/NFV MANO of the transport connectivity and network services for optical beamforming. The obtained experimental results show that the overall delay for the provisioning and removal of an OBF service, considering the contribution of the involved optical and radio systems and the SDN/NFV MANO layer, is 134 s and 18 s respectively. The reconfiguration of the OBF service to add or remove a beam can be performed in the range of 65–87 s.**

***Index Terms*—Optical beamforming, SDM, Fronthaul, SDN, NFV, 5G, beyond 5G, OBFN, ARoF**

I. Introduction

BEAMFORMING has been identified as a key technology for 5G and beyond to overcome the increased path loss at mm-wave and to increase the possible rate of frequency reuse by focusing the emitted energy in a confined area [1]. It enables to deploy remote radio heads (RRHs) with multiple beams that can be dynamically steered. However, electrical beamformers face challenges with regards to energy consumption, footprint and heat dissipation, causing multi-beam transmission with continuous steering of the beams to be a highly difficult task [2]. Additionally, the trend towards the centralized radio access network (C-RAN) architecture, where the signal processing of the baseband unit (BBU) is decoupled from the RRHs located at the cell sites (CSs) and moved to the central office (CO), introduces very stringent requirements in terms of high-bandwidth and low-delay in the fronthaul network [3]. Fronthaul is the network segment between the large centralized pool of BBUs at the CO and the RRHs, and it is traditionally used to transport digitally sampled radio waveforms to/from the CS [4]. The most widely used standard interface for the fronthaul is the common public radio interface (CPRI) and is deployed in optical fronthaul networks, making use of optical transceivers with digital radio over fiber (DRoF) solutions [5]. Optical fronthaul can be deployed with optical fibers assuring the connectivity between RRHs and centralized BBUs as studied in [6], or deploying wavelength division multiplexing (WDM) in passive optical networks (PON) architectures [7]. The main drawback of the C-RAN approach is that the massive MIMO antenna deployments foreseen in 5G will require huge bandwidth resources [8]. In order to reduce the bandwidth requirements of the fronthaul, and keep most of the benefits of the C-RAN architecture, the industry target a flexible functional RAN split for 5G, where some of the BBU functions are moved back to the RRH [9]. In this approach, the BBU functions are split into three logical entities; remote unite (RU), central unit (CU) and distributed unit (DU). It brings the introduction of the next generation fronthaul interface (NGFI) that is split into two network segments [10]. The fronthaul segment between the RU and DU is known as NGFI-I, and the network segment between the DU and the CU is the NGFI-II (also known as midhaul). This approach enables the packetization (e.g., Ethernet [11]) of the NGFI to provide more efficient network utilization in

Manuscript received February 1st, 2021; revised May 11th, 2021; published Mmm dd, ZZZZ. Work supported by the EC H2020 BLUESPACE (762055) and Spanish MICINN AURORAS (RTI2018-099178) projects.

R. Muñoz, C. Manso, R. Vilalta, J. M. Fabrega, R. Martínez and R. Casellas are with the Optical Networks and Systems Department of the Centre Tecnològic de Telecomunicacions de Catalunya (CTTC/CERCA), Castelldefels, Spain, e-mail: rmunoz@cttc.es, cmanso@cttc.es, rvilalta@cttc.es, jmfabrega@cttc.es, rcasellas@cttc.es, rmartinez@cttc.es,

S. Rommel and I. Tafur Monroy are with the Institute for Photonic Integration, Eindhoven University of Technology, Eindhoven, Netherlands, e-mail: s.rommel@tue.nl, i.tafur.monroy@tue.nl

J. Brenes and G. Landi are with Nextworks, Pisa, Italy, e-mail: j.brenes@nextworks.it, g.landi@nextworks.it

E. Grivas is with Eulambia Advanced Technologies Ltd., Athens, Greece, e-mail: egrivas@eulambia.com

C. Roeloffzen and P. van Dijk are with Lionix International, Enschede, The Netherlands, e-mail: c.g.h.roeloffzen@lionix-int.com, p.w.l.vandijk@lionix-int.com

ultra-dense scenarios (enabling the use of statistical packet multiplexing).

An alternative fronthaul solution deployed in the blue-SPACE project is to deploy optical beamforming (OBF) by combining space division multiplexing (SDM), analogue radio-over-fiber (ARoF), and the novel optical beam forming network (OBFN) technologies [12] [13], [14]. Spatial multiplexing is the key technology to overcome the capacity requirements for the 5G fronthaul transport between the RRHs and the BBUs [15]. The simplest way to deploy SDM is making use of the already deployed bundles of single mode fibers (SMFs), but the main goal is exploiting the spatial dimension of multi-core optical fibers (MCFs) [16]. On the one hand, ARoF transport supports reducing the bandwidth and latency requirements between the pool of BBUs and RRHs, where the desired radio waveform (or an intermediate frequency version, IFoF [17]) is directly transported over the fronthaul segment as an analogue signal, rather than in digitized form. Additionally, ARoF also contributes to the overall cost and reduced power consumption. The OBFNs can be compactly integrated due to the large wavelength difference between optical and RF signals [2], and placed at the CO, at the CS before the receiver, or at the CS after the receiver. Two OBFN variants have been proposed for investigation, namely the coherent and incoherent OBFN. The novel combination of OBFN technology with advanced ARoF solutions in SDM-enabled fronthaul infrastructures, allow the generation of multiple beams from a common antenna array at the CS. This is enabled by the parallel transmission of data streams over the space dimension in the up- and downlink (UL and DL) direction, thus simplifying the design requirements and reducing the size and energy consumption of the attached RRHs [18], [19].

From the service management point of view, advanced software defined networking (SDN) and network function virtualization (NFV) control and orchestration solutions are required to be developed with the goal to optimally manage and reconfigure the physical layer resources at the CO and CSs according to dynamically varying traffic models [12]. On the one hand, the control of the OBF fronthaul network is delegated to the optical SDN controller [20]. It is responsible for the lifecycle management (i.e., provisioning, reconfiguration and removal) of the OBF transport connectivity services. To this end, the SDN controller must be extended to configure and monitor the ARoF transceivers and the OBFN elements (both coherent and incoherent). On the other hand, the NFV orchestrator (NFVO) is responsible for the lifecycle management of the overall OBF network services. To this end, the NFVO must manage the analog BBUs and RRHs as physical network functions (PNFs) and embrace them as part of the orchestration domain, in contrast to the traditional NFVO platforms which are limited to the orchestration of common virtual network functions (VNFs) deployed in computing infrastructure. Additionally, the NFVO must also be seamlessly integrated with the SDN controller. It effectively enables to extend the orchestration domain towards the OBF fronthaul network. The proposed beyond 5G fronthaul architecture with dynamic optical beamforming services is primarily oriented to deploy massive machine-type communication (mMTC) services with dense deployment and high-bandwidth requirements, such as for industry 4.0, in contrast with other of mMTC-based use cases which provide large numbers of devices that intermittently transmit small amounts of traffic.

In this paper we present and experimentally validate for the first time the novel SDN/NFV-enabled fronthaul network for dynamic optical beamforming services. The main contributions of this paper are:

- SDM fronthaul system architecture with optical beamforming for beyond 5G networks.
- Incoherent and coherent 4x4 OBFN systems design and validation.
- SDN/NFV management and orchestration (MANO) architecture for dynamic optical beamforming services.
- Experimental validation of the provisioning, modification and removal of optical beamforming connectivity and network services.

The paper is organized as follows: Sec. II we present a use case of the proposed OBF fronthaul scenario for Industry 4.0. Then, Sec. III provides a description of the different implementation options considered for OBF fronthaul system architecture and the proposed SDN/NFV management and orchestration (MANO) layer. In Sec. IV, a detailed description of the deployed coherent and incoherent OBFN solutions are provided. Next, Sec. V presents the dynamic SDN/NFV management of the transport connectivity and network services for optical beamforming. Finally, the experimental validation is carried out in Sec. VI and Sec. VII concludes the paper.

II. Optical Beamforming Use Case for Industry 4.0

For the first time ever, 5G will offer reliable and secure wireless communications in real time and with low latencies, not only for humans but also for massive internet of things (IoT) providing pervasive and powerful connectivity. It will open new fields of applications in different vertical industries, such as Industry 4.0, automotive, energy, e-health, and media, becoming a driver for industrial and societal changes. IDC predicts that there will be 55.7 bn connected devices worldwide by 2025, 75 % of which will be connected to an IoT platform [21]. 5G will offer manufacturers the chance to build smart factories that will enable new operating models for Industry 4.0. Industry 4.0 aims at integrating IoT and the related services in industrial manufacturing and enable direct and seamless communication from the factories to the cloud for hosting industrial applications. Traditionally, cloud services have been implemented in large datacentres (DCs) in the core network. Cloud offers high computational capacity with moderate response time. However, there is a general trend to offer cloud service at the edge of the network (e.g., the CS or the CO). It is known as edge computing and leverages the low-latency and high-bandwidth transport connectivity services offered by fronthaul networks. For example, ETSI defines multi-access edge computing (MEC) [22].

The main focus of the Industry 4.0 use case is on the provision of services at factories with a large number of

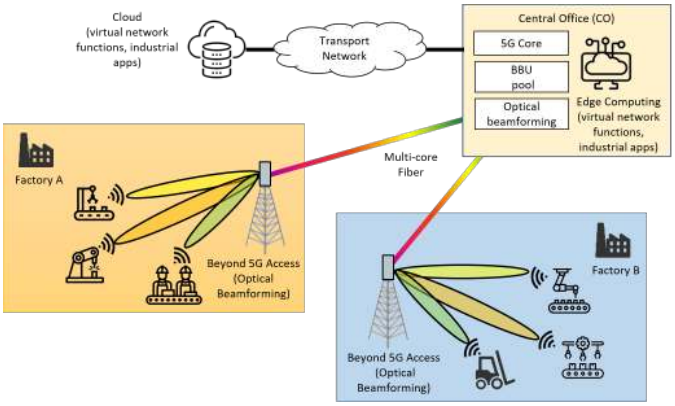

Fig. 1. Example of Industry 4.0 scenario with optical beamforming

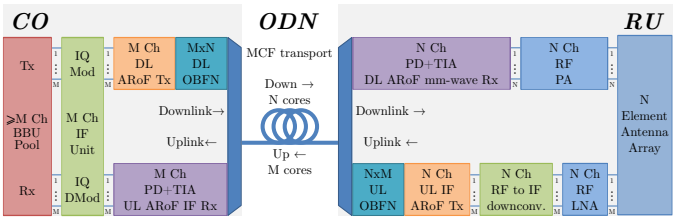

Fig. 2. Fronthaul system architecture with optical beamforming.

devices concentrated over certain plant areas. In contrast with other of mMTC-based use cases, this one considers also high-bandwidth applications that impose a huge requirements. The supported capacity requirement scales to 1 Gbit/s per aggregated group of devices and the connection density should be at least 100 devices/m^2 in this group or 10 000 users/RRH [23]. The information density should be more than 100 Gbit/s/plant and the end-to-end latency requirement is below 5 ms, although for some services it might be at the 1 ms level. These high-bandwidth and low-latency requirements are extremely challenging and can only be met by the beyond 5G fronthaul network with optical beamforming proposed in this paper.

Fig. 1 shows an example of the target Industry 4.0 use case deployed using the proposed OBF fronthaul network. It targets a mmWave small- and pico-cell environment for factories that exist within macro-cells, in a hybrid cell infrastructure. Each factory CS is equipped with a beyond 5G access antenna with mmWave beamforming and -steering for the different groups of aggregated devices in each plant. Spatial control of the signal is a key requirement to efficiently manage the spectral resources, maximize signal quality and minimize interference – despite the complex and dynamic environment. Optical beamforming has been suggested as an efficient alternative to electrical beamforming, enabling the shift from static and coarsely sectorized coverage to highly targeted and potentially dynamically steered beams [24], [25]. Broadband integrated optical beamformers for mmWave signals have been realized based on true-time delays and optical phase shifting [26], [27] and can be combined with focal plane arrays to improve gain while maintaining steerability [28], [29]. Their integration with optical transmitters and receivers as subsystems suitable for inclusion in a full beyond 5G system remains a challenge, as does the adaptation of the control and management plane.

Following the example in Fig. 1, the CSs are connected to the CO using a passive optical distribution network based on SDM. MCF is proposed for the SDM-based fronthaul segment to enable remote optical beamforming and to allow highly densified deployments with minimum fibre footprint. ARoF transceivers and OBFN elements are deployed at both the CSs and CO for ARoF transport and multi-beam transmission. Finally, a pool of BBUs with analogue input/output and edge computing servers are also deployed in the CO.

III. Proposed SDN/NFV-Enabled OBF Fronthaul Architecture

A. OBF Fronthaul System Architecture

The proposed 5G fronthaul system architecture employs ARoF transport and spatial multiplexing in MCFs and combines them with optical beamforming to achieve a flexible high-capacity mmWave fronthaul solution. The basic concept of ARoF fronthaul follows the C-RAN concept, centralizing signal processing for multiple RRHs at a CO and hence reducing their complexity and cost. The use of ARoF transport maximizes this centralization compared to traditional DRoF fronthaul approaches [18] and leaves only optical to electrical (O-E) conversion and RF amplification to be performed at the RRH. Together with the use of MCF it further alleviates the fronthaul capacity bottleneck faced by digital fronthaul technologies as carrier frequencies and radio bandwidths increase and the radio coverage strategy shifts from coarsely sectorized cells to highly targeted, beamformed signals or the use of massive multiple-input multiple-output (MIMO) signaling – both of which require large antenna arrays [30].

The proposed fronthaul architecture with OBF, as developed in blueSPACE, is shown in Fig. 2. A central pool of ARoF BBUs and intermediate frequency (IF) units performs all signal processing and waveform generation as well as up-/downconversion to/from IF. Notably, this centralizes the digital-to-analogue and analogue-to-digital conversion processes usually carried out at the RRH and, through tuneability of the IF local oscillator (LO), affords direct control and wide tuneability of the RF center frequency, while maintaining a fixed frequency for the mmWave LO.

For the DL signal, electrical to optical (E-O) conversion of the IF and signal preparation for mmWave generation by optical heterodyning are performed by an ARoF transmitter which first generates an optical two-tone signal using carrier suppression and 2nd harmonic generation in a Mach-Zehnder Modulator (MZM), before modulating the two-tone signal with the IF waveform. Optical heterodyning of the resulting ARoF signal would thus generate the desired RF signal at a frequency equal to the twice the frequency of the signal used in two-tone generation, plus the frequency of the IF, i.e., $f_{RF} = 2f_{LO,RF} + f_{LO,IF}$. Optical beamforming is performed by manipulation of the optical ARoF signal, creating multiple copies of the signal and either introducing differential phase shifts between the components of the two-tone signal to achieve differential phase shifts between the resulting RF signal copies or introducing differential time delays between the optical signal copies, resulting in differential time delays

between the RF signal copies. In both cases, the employed beamforming strategy – i.e., either phase shifting or true time delays – can be expanded into a multi-beam beamforming network allowing concurrent beamforming and -steering for M beams to be radiated from the same N-element antenna array.

In the proposed architecture, coherent beamforming is chosen for the downlink direction, as it provides maximum flexibility and fine-grained control over beam-direction and -shape, appropriate to maximize received signal quality and thus downlink channel capacity. The OBFN for downlink accordingly is an M×N coherent OBFN, which maps each of its M independent inputs onto each of its N antenna-side outputs, while introducing different progressive differential phase shifts, allowing the M input signals to be concurrently radiated as M independently steerable beams from the same N-element antenna array. While such an OBFN does provide maximum flexibility and true multi-beam transmission, its implementation is non-trivial (as discussed in Sec. IV) and its placement within the network has implications for the requirements on the transport segments. The latter arise from two factors: i) the M:N mapping performed by the OBFN which determines the number of parallel channels required for transport of the beamformed signal, and ii) the requirement that the relative phase between the N OBFN output signals be maintained until radiation from the antenna elements, as any phase shift would directly impact the resulting beam shape and direction. As a result, placement at the CO minimizes RRH complexity, but places stringent requirements on the availability of N parallel optical channels with matched propagation delay. Placement at the RRH, on the other hand, introduces significant complexity at the RRH, but removes the synchronization constraint and requires only M parallel transport channels.

As a result, the choice between centralized and remote beamforming strongly depends on the target network, in terms of required distances, available fibre counts and types and the number of beams and antenna elements. On the one hand, in a classical deployment scenario with substantial distances between RRH and CO and large antenna arrays with relatively few beams, placement of the OBFN at the RRH will be required, as maintaining phase synchronicity across more than a few km is challenging even when using MCF where, due to being contained in the same cladding, channels encounter less differential delays [31]. Similarly, the use of N fronthaul channels for M beams is not viable if N substantially larger M, i.e., relatively few beams are radiated from a large antenna array. On the other hand, in more densified deployments, where many smaller antennas are closely spaced and receiver density is large while the distance to the CO is small, placement at the CO may be preferable to minimize cost and complexity of the many RRHs. The latter case matches, for example, the Industry 4.0 use case deploying a private network where the CO is on-premise and a large number of RRHs are distributed to serve a high density of receivers requiring high network capacity. In these cases the number of beams per RRH will be more similar to the number of antenna elements and phase synchronicity over moderate distances can be achieved using MCF. blueSPACE has considered both cases and designed three OBFN and ARoF transmitter solutions: i) places the ARoF transmitter and OBFN at the CO, allowing direct integration between between ARoF Tx and OBFN and offering maximum centralization, at the cost of increased transport requirements, ii) places the OBFN at the RRH, transporting only the M independent ARoF signals to the RRH. Finally, iii) introduces an additional O-E-O conversion at the RRH, using IF-over-fibre transport and a fully integrated ARoF TX–OBFN–ARoF Rx assembly at the RRH – the latter is discussed in more detail in Sec. IV-A. In all cases, the final O-E conversion is performed by an N channel ARoF receiver, consisting of N photodiodes (PDs) for optical heterodyning and N trans-impedance amplifiers (TIAs). The RF signals are further amplified by N RF power amplifiers (PAs) and radiated from an N-element antenna array.

In the UL direction, the N signals received from the antenna are amplified and downconverted to IF, using a shared LO to maintain the relative phase. The resulting N IF signals are fed to the UL ARoF transmitter and OBFN which spatially filters the incoming signals for M different incidence angles and separates them onto its M different outputs. In the proposed architectures, incoherent beamforming is chosen for the UL, relaxing the requirements on the lasers in the UL ARoF transmitter and avoiding the need for further two-tone generation and optical heterodyne downconversion. For incoherent beamforming N independent lasers with a defined wavelength spacing are modulated with the N received IF signals and different differential true-time delays are employed in the OBFN when mapping the N antenna-side input signals onto the M output signals. Similar to the DL, synchronization of the signals must be maintained between the antenna elements and the beam side of the OBFN (in UL direction its output towards the CO) and scaling requirements on the number of parallel transport channels apply. Contrary to the DL case however, the output signals of the incoherent OBFN contain signal contributions from all N ARoF transmitter wavelengths, compared to only the two-tone signal derived from a single laser wavelength for the DL direction.

B. SDN/NFV MANO Architecture

The proposed SDN/NFV MANO architecture is shown in Fig. 3. It integrates an NFV service platform for the management of the complete OBF network services for verticals (e.g., Industry 4.0), a transport SDN controller operating the OBF connectivity services, an edge computing controller managing the computing infrastructure in the CO, and several SDN and PNF agents located and the CO and CSs for the configuration and monitoring of the deployed optical and radio systems (i.e., BBU, ARoF, OBFN and RRH).

The NFV service platform is composed of an NFVO, dedicated virtual network function manager (VNFM) and PNF managers (PNFMs), and a network slice manager (NSM) for vertical services. The NFVO manages the overall life cycle of the complete network services, by performing service function chaining of VNFs deployed in the edge computing

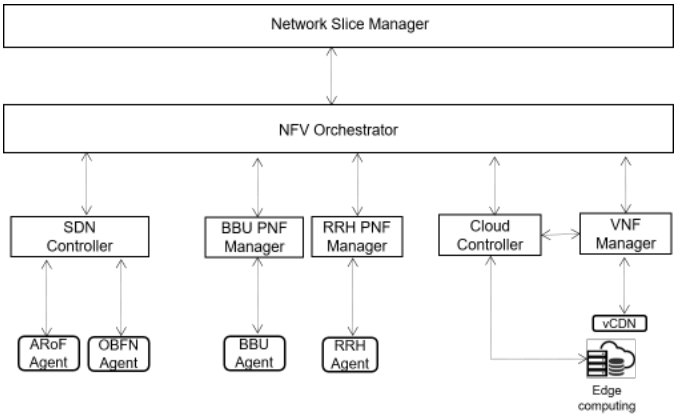

Fig. 3. SDN/NFV MANO architecture for the OBF fronthaul network

infrastructure at the CO, and PNFs from systems that cannot be virtualized, such as the pool of ARoF BBUs and RRHs. The NFVO coordinates the management of both VNFs and PNFs through the VNFM and PNFM respectively. The interaction with PNF equipment like RRHs and BBUs is mediated through the associated PNF agents, which translate standard messages from the PNFM into hardware-specific control commands. On the other hand, the interaction with the edge computing infrastructure is performed through the cloud controller. It acts as a virtual infrastructure manager (VIM), managing virtual machines (VMs) and virtual networks within the computing infrastructure. Finally, the NSM improves the efficiency in the utilization of fronthaul resources by enabling the delivery of multi-tenant virtual environments. It is deployed as a client of the NFVO and is responsible for the life cycle management of the network slice instances. It translates the vertical requirements into a suitable NFV network service with the required QoS which is instantiated and terminated at the NFVO [32].

The control of the OBF fronthaul network is delegated to the transport SDN controller, still under the global coordination of the NFVO. The communication between the NFVO and the transport SDN controller is based on the transport API (TAPI) [33], with extensions to deal with the specific optical beamforming technologies of the proposed fronthaul network, as described in Sec. V. The transport SDN controller manages the overall life cycle of the connectivity services in the OBF fronthaul network. It is extended with dedicated managers to configure and monitor the ARoF transceivers and the OBFN systems (both coherent and incoherent) through dedicated SDN agents using a REST API. The SDN agents are responsible for mapping the high-level operations in the REST API coming from the SDN controller into low-level, hardware-dependent operations.

C. SDN and PNF Agents

The ARoF BBU agents attach the ARoF BBUs to the SDN/NFV MANO layer through the ARoF BBU PNFMs, which allow the establishment of control parameters and the retrieval of monitoring information. The ARoF BBUs are responsible for the transmission and reception of the analogue signals that feed the ARoF transceivers. These signals are baseband extended 5G NR n258 [34] signals with a maximum bandwidth of 800 MHz, upconverted to a configurable IF at 2.25 to 5.5 GHz. The parameters of each ARoF BBU exposed to the blueSPACE control plane are: i) operational mode (5G NR numerology), ii) number of active subcarriers (4–3168, directly related to the bandwidth used), iii) modulation scheme (QPSK, 16-QAM, 64-QAM) and iv) IF frequency. In addition to the control parameters the following monitoring signals are supported by the BBU agent: i) measured EVM, ii) transmitter status and iii) receiver status. Each ARoF BBU requires an instance of an ARoF BBU agent and provides one DL and one UL channel.

The ARoF agent is responsible for passing the proper configuration to the ARoF transmitters (M for DL, N for UL) which are used to convert the IF signals from the electrical to the optical domain. The control parameters supported are the configuration of the wavelength and enabling/disabling the N lasers in the ARoF transceiver. It should be noted that when combined with a coherent OBFN, all lasers can be switched independently, while when combined with an incoherent OBFN, all lasers must be enabled jointly and their wavelength is defined by a starting wavelength for the first laser and a fixed grid for the remaining ones.

The OBFN agents enable the SDN controller to control the beam-steering functionality offered by the OBFNs. The SDN controller specifies the reference wavelength and, for each beam, the information regarding horizontal and vertical offset angles (ranging from −60 to 60°) and the width (ranging between 20 and 60°). The OBFN agent translates these to a set of parameters π_j, ϕ_j, with j ranging from 1 to the number of antenna elements N, so that the π_j correspond to the relative power fed to antenna element j, while the ϕ_j correspond to the respective relative phase. The π_j determine beam broadening and coverage optimization, while the ϕ_j are related to beam focus and directional properties. These sets of parameters are then used to control the tuning elements of the OBFN (108 in the case of a 4x4 OBFN) to achieve the beamforming functionality as previously described.

The RRH agent bidirectionally communicates with the respective PNFM and is responsible for the configuration of the hardware components present in the RRH, such as the power amplifiers, and for providing several monitoring parameters back to the SDN/NFV MANO to aid the selection of the RRHs and the configuration parameters required to serve one network service. The control parameters supported by the RRH agent are: power up, power amplifier i gain, where $i \in [0, N-1]$. Each RRH requires an instance of an ARoF RRH agent.

IV. Incoherent and Coherent OBFN Systems

This section introduces the coherent and incoherent OBFNs designed and manufactured in blueSPACE to implement the OBF fronthaul architecture discussed in Sec. III-A.

A. Coherent 4×4 OBFN

This OBFN module, a hybrid indium phosphide (InP) and silicon nitride (TriPleX) assembly, comprises the following on-board functions from the active InP components:

1) An InP modulator array PIC. The half wave voltage of the modulator V_π is 3 V up to a frequency of 40 GHz.
2) Two InP gain (reflective semiconductor optical amplifier, RSOA) chips with optical an output power of >40 mW. A linewidth of <1 kHz and tuneablity over the entire C-band, are established through use of an external micro-ring resonator mirror in TriPleX.
3) A PD array with internal biasing and a responsivity of 0.6–0.8 A/W for frequencies up to 40 GHz. The PD chip needs external 50 Ω impedance matching.

The TriPleX processor, depicted in Fig. 4 comprises a relative intensity noise (RIN) suppression filter with a free spectral range (FSR) of 18 GHz and containing three tuning elements [H5, H6, H7] and two tuneable couplers (TCs) [H5, H6] used to change the quality of the filter, or to completely bypass the filter by putting both switches in 'cross' state. This ring filter suppresses the spontaneous noise of the laser at the position of the signal sidebands prior to the modulation in the phase modulators (PMs).

The frequency of the drop response can be tuned with the heater on top of the ring [H7]. The light is then directed towards the two TCs [H8, H9]. With the first coupler external light [FA17] can be added from an optical fiber, or the internal laser light can be directed into this optical fiber. This feature is conveniently used for initial setup and for testing purposes. When the TC (switch) is placed in 'bar'-state, the light is directed to the second switch that directs the light ('bar') to either the 1×4 splitter before the modulators or ('cross') optionally and partially to the 'carrier re-insertion (CRI) port. The 1×4 splitter splits the light equally up to the 4 phase modulators. This splitter is fully configurable and all the optical power can also be directed to one of the four modulators. The modulated light is fed through path-length compensation blocks before it is directed to the Blass matrix. Each node of the matrix consists of a tuneable 2×2 switch and additional phase shifter. In this way a fully tuneable 4×4 Blass matrix is realized. The switches in the matrix can also be set to full 'cross' or 'bar' state. This provides a controlled guidance of the light to the individual integrated single sideband (SSB) filters and connected PDs. The waveguides at the north and east side of the Blass matrix are also directed to the fibre array for monitoring and testing purposes. The signals at the four outputs of the Blass matrix are directed towards the 2×2 optical sideband filters, where both the original carrier (C) and lower sideband (LSB) signal are suppressed and the new carrier, from the second laser (labelled OPTIONAL in Fig. 4), is re-inserted. It is also possible to re-inject the original carrier from the main laser (laser 1). Finally, the four SSB+C signals are directed to the four photodiodes [PD1–PD4] and mixed back to the RF signal at the output. The complimentary optical output ports of the SSB filters (labelled OSSB) are fed to the fiber array for monitoring. In total, the integrated 4×4 OBFN has 40 fiber in- and outputs.

The TriPleX processor chip has 82 heaters to configure the TCs. Unfortunately, the heaters create an insurmountable heat dissipation problem, resulting in thermal crosstalk, especially in close proximity typically within 250 µm. To reduce the effect of the thermal crosstalk for neighboring waveguides in the proximity of each heater, the integrated 4×4 OBFN is placed on top of a temperature controller/thermoelectric cooler (TEC) which is set to 35 °C during measurements, hereby establishing a stable and conditioned reproducible operational configuration. The size of the complete 4×4 OBFN assembly is 110×70 mm and is depicted in Fig. 5.

Once the OBFN is fully assembled, several performance pre-checks are performed, including analog optical link measurements. In particular the following are verified, measurements for the most important of these are discussed in Sec. VI:

- Electrical resistance of the heaters are measured ($461 \pm 7\,\Omega$);
- Diode voltages are measured (within 3 % from applied voltage);
- Optical power losses are measured between different interfaces (<1.5 dB/facet);
- Cross and bar voltages/power are determined (power difference between cross and bar is 380 ± 83 mW for a total of 22 switches);
- Lasers are tuned to check functionality: typical output power 8.5 dBm at 250 mW applied current; the frequency difference of two laser is set to 22 GHz for operation;
- RIN filter responses are measured;
- Phase modulator responses are measured;
- Filter responses are tuned;
- Photocurrent and PD responses are measured.

B. Incoherent 4×4 OBFN

The ARoF uplink comprises three separate physical parts:

1) This 4 λ transmitter, used as an optical source, located at the CS;
2) The incoherent 4×4 OBFN also at the CS;
3) The four-detector array assembly, located at the CO.

The incoherent 4×4 TriPleX OBFN is considered as the UL beamforming solution. It is a monolithic (TriPleX-only) beamformer, distributing independent wavelengths ($\lambda1$–$\lambda4$) to four output ports (A, B, C, D), applying incremental incoherent true-time delays per wavelength per port. Moreover, it incorporates twelve TCs and optical filters in the four sections (α, β, γ, δ), as depicted in Fig. 6

The 14×16 mm OBFN PIC comprises several filters: 1600 GHz asymmetric Mach-Zehnder interferometers (aMZIs) (8×), 800 GHz aMZIs (4×), and switches: MZIs (12×). The 'cross' and 'bar' states of each MZI are determined by the calibration procedure of the signals at the output ports for maximum and minimum signal propagation respectively. All optical in-/output path lengths are kept equal by design. Note that there are nine waveguide crossings in the chip-layout, an unavoidable solution to meet the functionality requirements of the OBFN. Moreover, on-chip spot size converters, or tapers, are introduced to meet the mode-field dimensions of the fibers at the interface and alignment loops for optical interfacing are assigned to the two outer ports at each location of the twelve-port multi-fiber push on (MPO) connector.

The twenty four electrical pads (North/South) provide access to the heaters, comprised of 800 Ω Cr/Pt resistors, positioned above the optical waveguides, to control and tune the

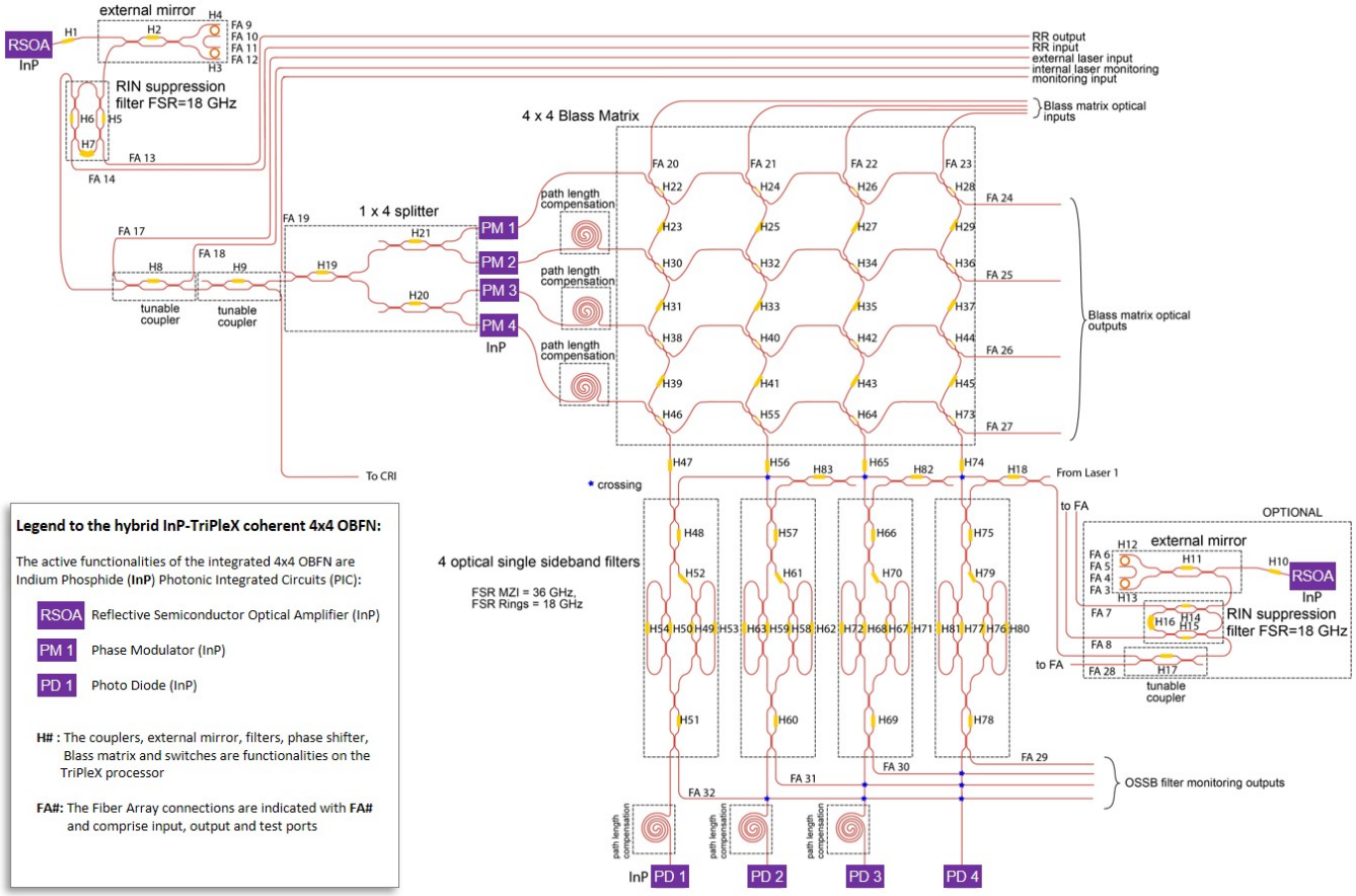

Fig. 4. Detailed functional schematic of the coherent integrated 4x4 OBFN with integrated dual laser, modulator array and detector array, including labels of the heater actuators.

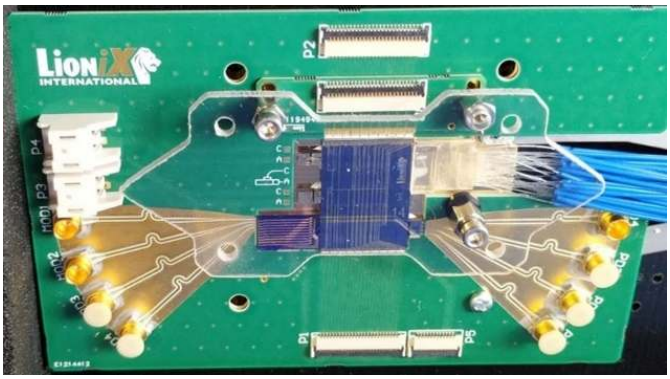

Fig. 5. Full assembled integrated coherent 4×4 OBFN. The fiber array (40 fibers with light blue shielding) is used for characterization and monitoring of the different building blocks of the module.

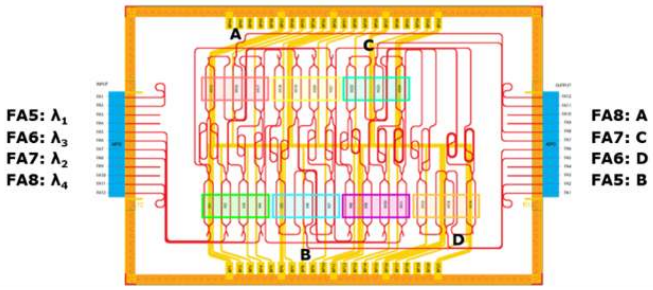

Fig. 6. Mask layout of the incoherent 4×4 OBFN, used in the blueSPACE uplink (left=input, right=output).

on-chip MZIs, also referred to as TCs. All microwave photonic (MWP) measurements on the incoherent 4×4 OBFN have been performed using a tailored control unit, which provides control signals for the 'heaters' while the temperature of the PIC is stabilized at 30 °C through a TEC. The incoherent 4×4 OBFN requires two PCBs to route the DC leads to and from the heaters on the TriPleX chip. The interface connectors are industry standard 51-pin connectors with 0.3 mm pitch. The 3D assembly in Fig. 7 includes a 200 g gold plated copper mount (52×52 mm), which holds the PCBs, the PIC, and the supports for the optical fibers which are coupled to the optical chip by the MPO connectors.

The 4 λ transmitter, depicted in Fig. 8, is used as an optical source for the four RF inputs of the incoherent 4×4 OBFN to establish the UL to the detector array at the CO. The assembly incorporates a TriPleX interposer that acts as a pitch and spot size converter and interfaces between the ARoF InP chip and the fiber array with MPO connector. Additionally, path length compensation has been added to the TriPleX chip. The mode profiles in the waveguides and the angle and pitch of the

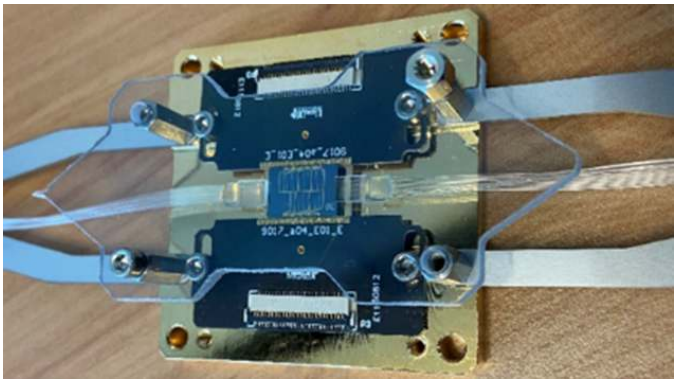

Fig. 7. Incoherent 4×4 OBFN with MPO input at the right and output at the left, DC PCBs at top and bottom.

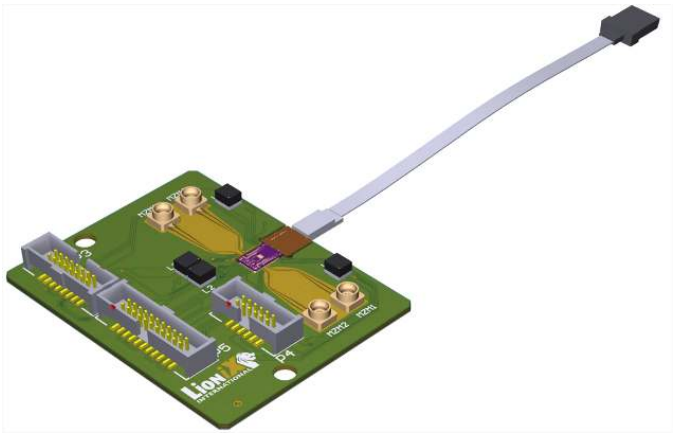

Fig. 8. Isometric 3D render of the 4 wavelength transmitter as used for the incoherent 4x4 OBFN. The size of the assembly is 40×49.8 mm.

Fig. 9. Top: Photograph of a four-detector array attached to the TriPleX interposer and the four-TIA chip as well as output PCB RF lines (before wire bonding). Bottom: Two complete detector array assemblies with MPO connector, differential RF outputs and on-board TIAs.

waveguides at the west side of the chip are matched to the InP chip, and at the east side of the chip to the fiber ribbon cable.

The third module of this UL is the four-detector assembly with differential RF out-puts. The on-board TIAs are the MACOM Quad Linear 28 GBd MATA-03819. A TriPleX interposer is used to interface the detector array chip to the fiber ribbon cable and is part of the four photodiode module and again optical pathlength equalization has been performed on the TriPleX chip. Fig. 9 shows a close up of the InP detector array connected to the TriPleX interposer (left-most chip), the array of four TIAs and RF-transmission lines on the PCB (top) and two complete assemblies (bottom).

V. Dynamic Optical Beamforming Services

A. SDN OBF Connectivity Service

The interface between the NFVO and the SDN controller is based on the TAPI specification [35]. We have defined a new TAPI data model for the OBF transport connectivity service (tapi-obfn.yang) [36]. For this, an additional protocol layer qualifier *tapi-obfn:PHOTONIC_LAYER_QUALIFIER_OBFN* within the *PHOTONIC_MEDIA* layer has been introduced. The model augments key TAPI entities and objects in support of optical beamforming.

In general, the SDN controller generates a TAPI context for the NFVO. A TAPI context is defined by a set of service interface points (SIPs), which enables the NFVO to request connectivity services between pairs of endpoints to the SDN controller. Fig. 10 shows an example of the TAPI context provided by the SDN controller to the NFVO. In particular, SIPs are augmented with the supported wavelength band and grid, the supported number of beams (e.g., four), the supported upper and lower angle (e.g., 60°, −60°), and the supported max and min width (e.g., 60°, 20°). Additionally, a TAPI context may also expose an abstract topology. In the example of Fig. 10, the topology is composed of a single node with two node edge points (NEPs) acting as node ports. Each NEP is mapped to two SIPs, one associated to the DL and another to the UL.

The topology information is updated for each connectivity service call. In particular, the NEPs are updated with a list of connection end points (CEPs). CEPs encapsulate information related to the provisioned connection. The connectivity service request call and the CEPs are augmented with the requested/configured reference wavelength, and a list of beams, specifying for each beam the status (on/off), the X and Y offset angles, and width. It is worth highlighting that for the coherent OBFN (i.e., DL), each channel of the ARoF transmitter corresponds to one beam and all share the

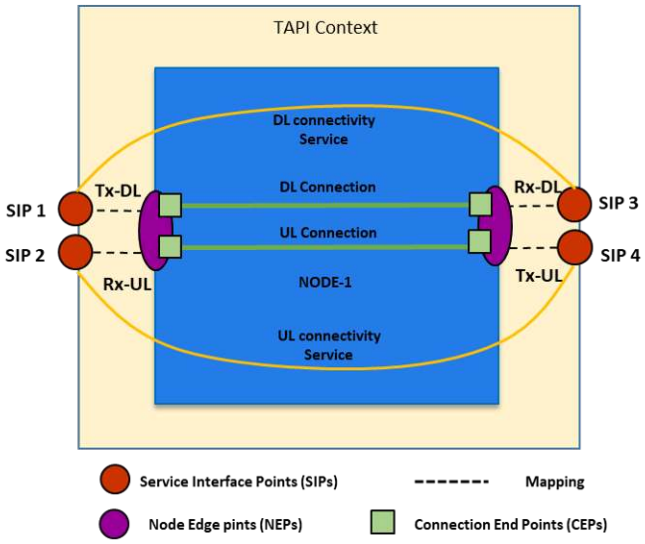

Fig. 10. Example of TAPI context for optical beamforming.

same wavelength. For the incoherent OBFN (i.e., UL) all channels are always activated and are separated by 200 GHz. We consider unidirectional connectivity services, therefore the OBF connectivity service parameters for the downlink and uplink are defined separately in two different calls. In general, the NFVO can request the provisioning of a TAPI OBF connectivity service for the DL/UL that is composed of one or several beams. Once the OBF connectivity service is provisioned, the NFVO can also request to add new beams, remove or reconfigure existing beams of the provisioned OBF connectivity service. Finally, the NFVO can also request to remove the whole OBF connectivity service.

Fig. 11 shows an example of a complete workflow between the NFVO, SDN controller and the SDN agents for the provisioning, reconfiguration and removal of an OBF connectivity service. In the first step, the NFVO requests the provisioning of a DL/UL OBF connectivity service (TAPI POST connectivity service) with the associated beamforming parameters between a pair of SIPs. An example considering only beam 1 active is reference wavelength 197.900 GHz, beam-1 with X offset angle 60°, Y offset angle 40° and width 20°, and beam 2 to 4 disabled. The optical SDN controller maps the SIPs to the involved ARoF and OBFNs and requests the configuration through the respective agents. First, the optical SDN controller configures the 4×4 coherent and incoherent OBFNs (for DL/UL respectively) with the associated parameters for beam 1. Then, the SDN controller either configures the ARoF transceiver at the CO by configuring the wavelength and turning on laser 1 for the DL connectivity service request, or the the ARoF transceiver at the CS by configuring all four lasers on for the UL connectivity service request. These four wavelengths are spaced by 200 GHz each, starting with the specified reference wavelength. After configuring all optical systems, the SDN controller updates the TAPI context by adding one CEP in each NEP associated to the source and destination SIPs. CEPs provides information of the configured parameters for the provisioned DL/UL OBF connection. Then,

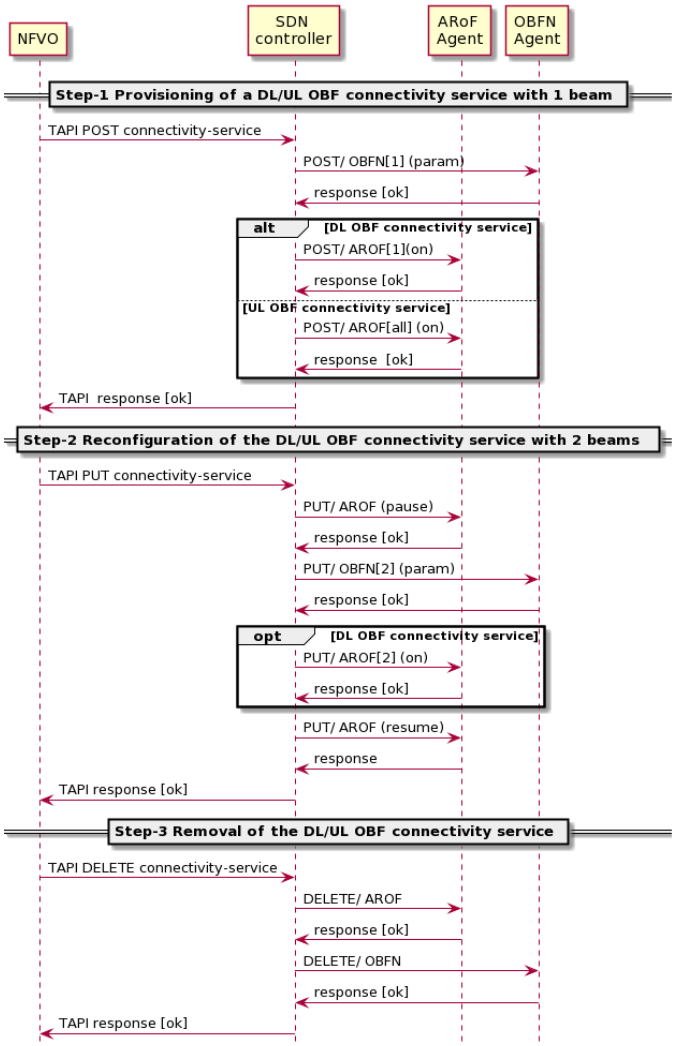

Fig. 11. Workflow for the provisioning and reconfiguration of an SDN OBF connectivity service

the SDN controller saves the information of the DL/UL OBF connection and the DL/UL OBF connectivity service in the service database, and sends a TAPI connectivity service response to the NFVO.

In the second step, we reconfigure the DL/UL OBF connectivity services. The NFVO requests the reconfiguration of the provisioned DL/UL OBF connectivity service by adding a second active beam with the associated configuration parameters (e.g., beam 2 with X offset angle 20°, Y offset angle −20° and 40°). First, the SDN controller requests to pause the ARoF transceiver by disabling all lasers at the CO for DL or CS for UL. Then, the SDN controller reconfigures the 4×4 coherent/incoherent OBFNs by adding the parameters for beam 2. For the reconfiguration of the DL connectivity service, the SDN controller requests to turn on laser 2 to the ARoF transceiver located at the CO. Finally, the SDN controller request to resume the corresponding ARoF transceiver at CO or CS (for DL/UL respectively), enabling all lasers that where configured as on. Once the DL/UL OBF connectivity service is reconfigured, the SDN controller updates the CEPs in the TAPI context associated to the DL/UL OBF connection with

the new parameters for beam 2.

In the third step, we remove the overall DL/UL OBF connective service. The NFVO requests the SDN controller to remove the DL/UL OBF connectivity service. The SDN controller requests to disable all lasers in the corresponding ARoF transceiver at CO or CS (for DL/UL respectively) and all beams in the coherent/incoherent OBFNs, and removes the associated information in the respective SDN agents. Finally, the SDN controller removes the CEPs associated to the DL/UL OBF connections, as well as the information of the DL/UL OBF connectivity service and connection in the service database.

B. NFV OBF network service

Fig. 12 shows the workflow involved in the instantiation of a complete NFV network service in the OBF fronthaul, involving the BBUs and RRHs. Before the instantiation, it is required to create a network service descriptor (NSD), containing references to the descriptors for RRH and BBU PNFs. After the successful onboarding of the NSD, the instantiation procedure can start by means of a network service (NS) instantiation request. Upon receiving an instantiation request, the NFVO computes the resource allocation solution using the resource allocation algorithm (RA). The NFVO then feeds the RA with the service constraints and the infrastructure resource information including the information retrieved from the SDN controller. The outcome of the RA determines the OBFN resources (i.e., reference wavelength, and offset angles and width for each beam to setup the OBF connectivity service) and the RRH and BBU devices to be used and their configuration parameters. The following step involves the configuration of the RRH, which is configured through the RRH PNFM with the settings selected by the allocation algorithm (e.g., the PA gains). The PNFM sends the configuration to the correspondent RRH PNF agent, which in this scenario controls four RRHs.

Once the RRH is configured, the NFVO requests the provisioning of the OBF connectivity service for the downlink and uplink. For this, the NFVO selects the SIPs associated to the involved BBUs and RRHs and issues two TAPI POST connectivity service request for the downlink and uplink, containing the selected SIPs, the obtained reference wavelength and the array of the offset angles (X and Y) and width for each beam. The optical SDN controller maps the SIPs to the specific ARoF and OBFN devices and starts the configuration through the respective agents, as shown previously. Once both the downlink and uplink OBF connectivity services are provisioned, the NFVO configures the involved BBUs through the BBU PNFM that send the corresponding configuration (e.g., 5G NR waveform parameters provided by the resource allocation) to the BBU PNF agent. It is required to configure as many BBUs as beams are activated. At this point, OBF NFV network service is instantiated.

The next step in the workflow is to modify the established OBF NFV network services to add new beams or remove existing ones. If new beams are requested, the NFVO requests to the resource allocation algorithm the information of required

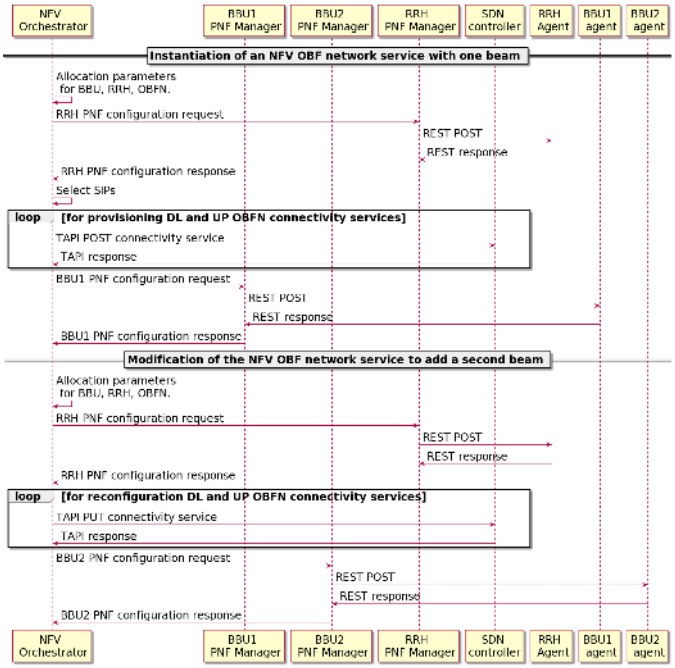

Fig. 12. Workflow for the provisioning and reconfiguration of an NFV OBF network service

resources and updates the RRH configuration. Then, the NFVO requests to the SDN controller the modification of the existing OBF connectivity services, both for the downlink/uplink, specifying the new configuration of the beams in the TAPI connectivity service. The optical SDN controller configures the coherent/incoherent OBFN devices with the new beams, and the ARoF transceivers at the CO and CSs. After that, the NFVO configures the required BBUs and establishes the network service as completely instantiated.

VI. Experimental Setup and Results

This section first discusses the characterization of the OBFN modules, before detailing the validation of the deployment, reconfiguration and removal of dynamic OBF connectivity and network services though the SDN/NFV MANO layer and providing results for the time required for each included in the workflows discussed in Sec. V.

A. Validation of Coherent and Incoherent 4×4 OBFN Systems

For the driving of the OBFN assemblies, dedicated driving electronics were developed, available in an industry standard 19-inch rack, including a USB interface to a PC and control software, which can be used to fully tune the TCs/phase shifters/switches on the assembled PIC. The driver board solution provides is modular and scalable and is aimed for lab-based characterization of a variety of complex assemblies of PICs. Each of the electronic boards, connected to the device under test by flat ribbon cables from the DUT as depicted in Fig.13, has a USB-to-serial chip on-board to translate the messages to and from the microprocessor on the PCBs. A graphical user interface (GUI) has been developed to translate

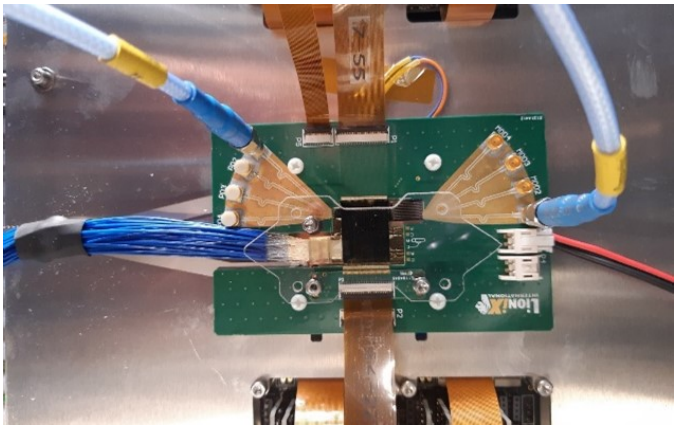

Fig. 13. The integrated 4×4 OBFN mounted in the 19-inch control unit with two RF cables connected to phase modulator MOD1 and photodiode PD4.

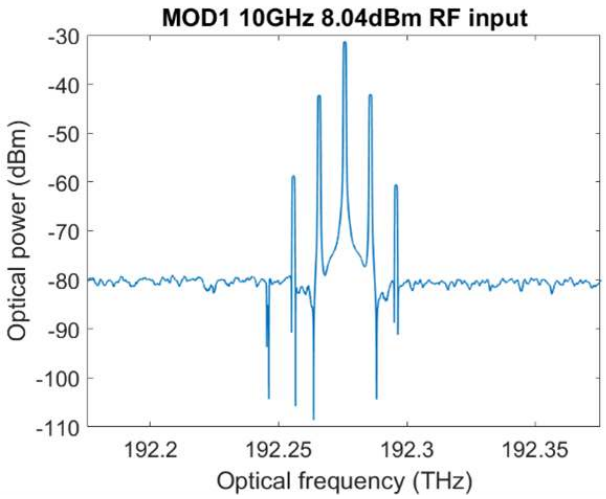

Fig. 14. Optical response of at 8.73 dBm 10 GHz RF input (averaged 32 times).

setting and monitoring values to serial command messages and back, simplifying control of the OBFN.

For characterization of the integrated coherent OBFN, the fiber array is used as auxiliary I/O of the TriPleX chip. A vector network analyzer (VNA, Keysight N5244B PNA-X) is used to generate and measure RF signals and a Finisar Wave Analyzer 1500S is used to measure and optical spectrum at the fiber output. The initial pre-checks of MWP functions and measured performance of the coherent integrated 4×4 OBFN provided results form measurements up to 40 GHz. The half-wave voltage $V\pi$ of the phase modulators is typically 1.7 V at 5 GHz and 3.0 V at 30 GHz and the optical response of each modulator is comparable. A typical response curve of the modulator at 8 dBm 10 GHz RF input is depicted in Fig. 14.

The four SSB filters are tuned to a fifth order filter. Each filter must have the stop and pass band at the same position in the RF and optical domain. For these measurements, an external tuneable laser, sweeping from 1558.8880 to 1559.4717 nm (central wavelength 1559.18 nm ± 36 GHz FSR), is used. The light is modulated by a MZM with an RF input of −5 dBm at 100 MHz. The output of the MZM (3.67 dBm) was used

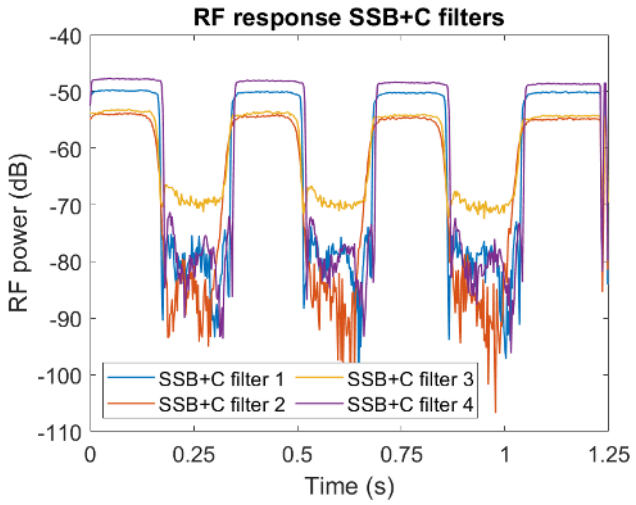

Fig. 15. RF filter responses of the four SSB filters on the TriPleX chips.

as input at fiber 8 to the TriPleX chip. The laser triggered the VNA to measure the photodiode response in the time domain. The measured FSR is 36 GHz and the suppression of the stopband of SSB+C filters 1 and 4 is 30 dB, for SSB+C filter 2 the suppression is 25 dB and for SSB+C filter 3 the suppression is 15 dB, as seen in Fig. 15.

The stability of the RF link performance was measured by setting up a 1-to-2 network (MOD4-PD4/MOD4-PD1) and is depicted in the top graph of Fig. 16. Although the observed power was stable, the phase at the PDs fluctuates significantly within a time window of 10 s. Although these fluctuations are unexpected and disturbing, for proper operation of the beamformer the relative phase fluctuations are more important. The latter can be measured by setting up a 2-to-2 network: the signal from the laser is now split into two paths, directing the light equally from MOD4 to PD1 and from MOD3 to PD4, both connected to the VNA, and the transfer functions are measured simultaneously. The CRI is also split and equally divided over the two PDs. The bottom graph of Fig.16 shows that both optical paths have equal phase fluctuation.

A substantial common phase drift in the APLs of the OBFN would not result in degradation of the beamforming because the direction/shape of the beam is determined by the relative phases. The fluctuation is also too slow to degrade the quality of the transmitted symbols in the communication link. However, it is not known what the origin of the power fluctuation is and why its shape is similar to the phase fluctuation. The signal and carrier follow separate paths and are combined in the SSB filter, while the unwanted LSB and much lower power carrier from the modulator are suppressed by at least 20 dB. Further investigation is needed to find the cause of the power and phase fluctuations where we consider contributions from a) large path length difference between the signal path and the CRI path together with frequency fluctuation of the laser and b) temperature fluctuation of the assembly.

The individual modules for the incoherent OBF UL – 4 λ transmitter, incoherent OBFN and PD+TIA array – have been characterized and are currently being implemented in the blue-

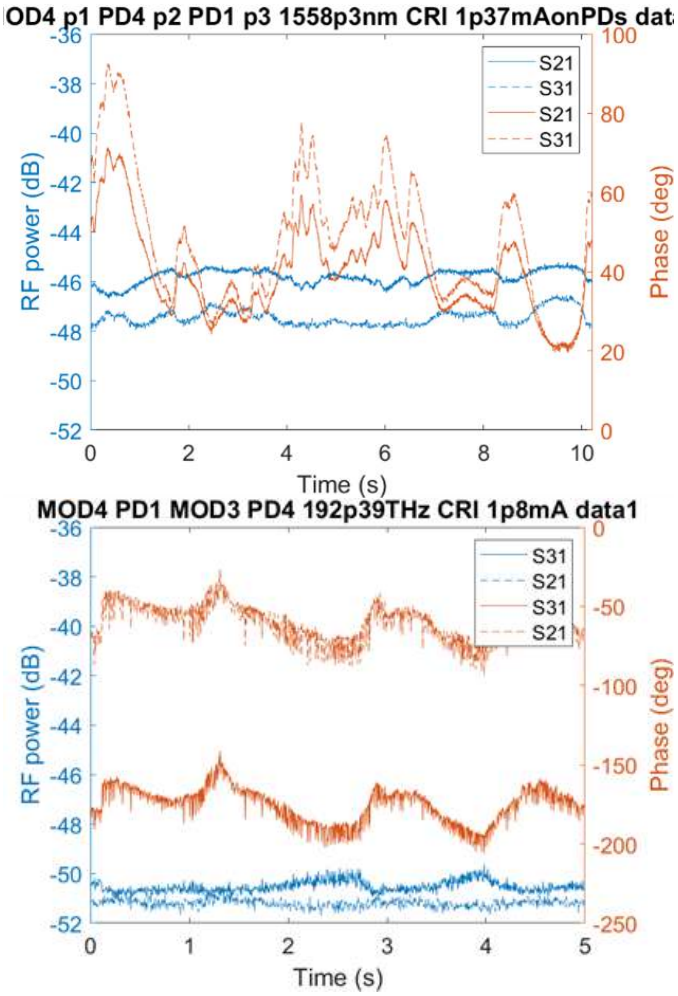

Fig. 16. RF link stability test. Top: SSBSC with CRI from modulator 4 to detector 1 and 4. The average photocurrent is 1.4 mA. Bottom: SSBSC with CRI from modulator 4 to detector 1 and from modulator 3 to detector 4. The average photocurrent is 1.8 mA.

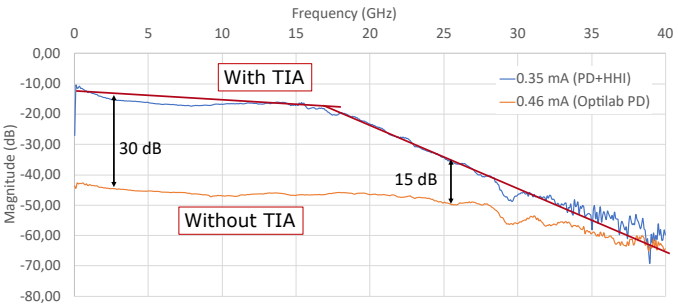

Fig. 17. Magnitude response of the PD+TIA assembly compared to an Optilab high speed PD from 0 to 40 GHz.

SPACE testbed. Fig. 17 shows the magnitude response of the PD+TIA assembly from 0 to 40 GHz. The measured response is 25–30 dB higher than the reference (Optilab PD-40-M) for frequencies up to 15 GHz with a slope of −0.4 dB/GHz. The slope is 2 dB/GHz for higher frequencies. The PD chips have been measured separately and no roll-off was observed up to 40 GHz, this roll off should thus be caused by the limited bandwidth of the employed TIA chips.

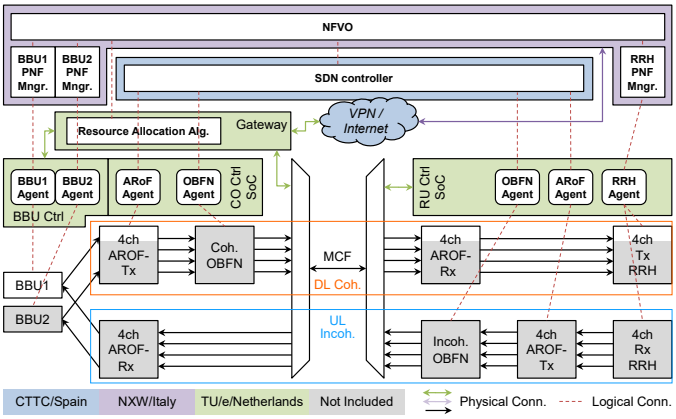

Fig. 18. Experimental setup, including the SDN and NFV control and the OBF fronthaul.

B. Validation of Dynamic OBF Connectivity and Network Services

Fig. 18 shows the experimental scenario deployed for the validation and evaluation of OBF connectivity and network services. The different SDN and NFV control are orchestration systems are deployed in a geographically distributed fashion, with the the SDN controller in Barcelona (CTTC), the NFVO and BBU/RRH PNF managers in Pisa (Nextworks), and the SDN/PNF agents and resource allocation algorithm service in Eindhoven (TU/e). The agents are deployed on system-on-chip boards ready for direct integration with the ARoF BBUs, ARoF fronthaul transmitters, OBFNs and RRHs. The different locations are connected to the CTTC premises using open virtual private network (VPN) tunnels through an open VPN server. On the TU/e side, a gateway provides connectivity and routing towards all SDN/PNF agents and a fibre-based control channel between the CO and RU ensuring control connectivity across the fronthaul link.

The fronthaul hardware included in this experimentation implements a single ARoF DL channel, including the ARoF BBU, the ARoF transmitter, the MCF transport and the RRH and is deployed in the testbed at TU/e. The ARoF transmitter consists of a narrow-linewidth laser, a high-bandwidth MZM for two-tone generation, an optical amplifier and a second MZM for modulation with the IF signal. MCF transport is performed over 10 km in a 7-core MCF, with the ARoF signal in the optical C-band and the bidirectional control channel in the O-band multiplexed on the same core. A second core is employed to feed a copy of the two-tone signal to the RRH to be used as LO for downconversion of the UL signal [37].

We have performed two different validation tests. In the first validation test, we have fully assessed the proposed SDN/NFV MANO architecture without hardware. In this scenario, we used dummy agents that were not connected to the actual hardware. We have tested and measured, from a control perspective, the overall OBF connectivity and network service delay for four testing scenarios:

1) Provisioning of an OBF network service with one beam;
2) Modification of the OBF network service by adding a second beam;

a) OBF NFV network service provisioning

```
*REF*     NFVO    SDNc    HTTP    POST /restconf/config/context/connectivity-service/
0.890503  SDNc    NFVO    HTTP    HTTP/1.1 200 OK  (application/json)
0.909792  NFVO    SDNc    HTTP    POST /restconf/config/context/connectivity-service/
23.654582 SDNc    NFVO    HTTP    HTTP/1.1 200 OK  (application/json)
24.512001 NFVO    RRHa    HTTP    PATCH /vnfconfig/v1/configuration HTTP/1.1  (applic
24.512365 NFVO    BBUa    HTTP    PATCH /vnfconfig/v1/configuration HTTP/1.1  (applic
26.862063 RRHa    NFVO    HTTP    HTTP/1.1 200 OK  (application/json)
38.117364 BBUa    NFVO    HTTP    HTTP/1.1 200 OK  (application/json)
```

b) OBF SDN DL connectivity service provisioning

```
*REF*  NFVO   SDNc    POST /restconf/config/context/connectivity-service/8f6e757a-aa57-498e
0.661  SDNc   Agents  POST /arof HTTP/1.1 , JavaScript Object Notation (application/json)
19.825 Agents SDNc    HTTP/1.0 200 OK , JavaScript Object Notation (application/json)
19.884 SDNc   Agents  POST /obfn HTTP/1.1 , JavaScript Object Notation (application/json)
19.973 Agents SDNc    HTTP/1.0 200 OK , JavaScript Object Notation (application/json)
20.036 SDNc   NFVO    HTTP/1.1 200 OK , JavaScript Object Notation (application/json)
```

c) OBF NFV network service removal

```
*REF*     NFVO    SDNc    HTTP    DELETE /restconf/config/context/connectivity-service/
0.785975  SDNc    NFVO    HTTP    HTTP/1.1 200 OK  (application/json)
0.791594  NFVO    SDNc    HTTP    DELETE /restconf/config/context/connectivity-service/
2.735691  SDNc    NFVO    HTTP    HTTP/1.1 200 OK  (application/json)
2.740361  NFVO    SDNc    HTTP    GET /restconf/config/context/ HTTP/1.1
2.825669  SDNc    NFVO    HTTP    HTTP/1.1 200 OK  (application/json)
5.721740  NFVO    RRHa    HTTP    PATCH /vnfconfig/v1/configuration HTTP/1.1  (applica
7.542777  RRHa    NFVO    HTTP    HTTP/1.1 200 OK  (application/json)
```

d) OBF SDN DL connectivity service removal

```
*REF*  NFVO   SDNc    DELETE /restconf/config/context/connectivity-service/8f6e757a-aa57-498e
0.312  SDNc   Agents  DELETE /arof HTTP/1.1
1.555  Agents SDNc    HTTP/1.0 200 OK , JavaScript Object Notation (application/json)
1.612  SDNc   Agents  DELETE /obfn HTTP/1.1
1.699  Agents SDNc    HTTP/1.0 200 OK , JavaScript Object Notation (application/json)
1.833  SDNc   NFVO    HTTP/1.1 200 OK , JavaScript Object Notation (application/json)
```

Fig. 19. Packet captures for OBF connectivity and network service provisioning and removal.

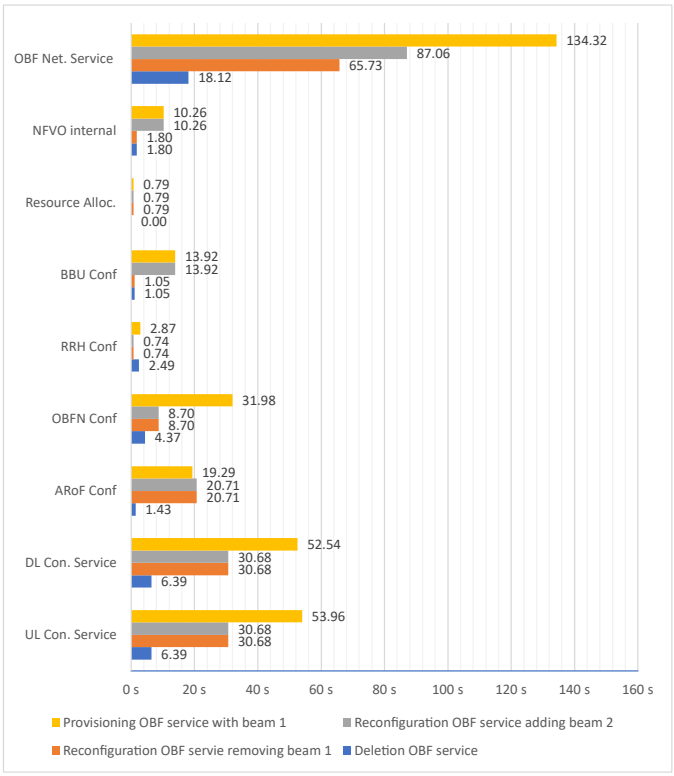

Fig. 20. Measured OBF network service delay and component contributions.

3) Modification of the OBF network service by removing the first beam;
4) Removal of the OBF network service.

In the second validation test, we partially integrated the proposed SDN/NFV MANO architecture with the available hardware as described in Fig. 18. We performed several measurements of the hardware configuration time, in order to estimate/extrapolate the contribution of the hardware in the four scenarios previously addressed. In particular, we considered an OBF network service composed of one beam, involving the real BBU, RRH, and ARoF transceiver for downlink. As an example of the measured data, Fig. 19 a) and c), show the packet exchanges between the developed NFVO, the SDN controller and the RRH and BBU agents to provision and remove the OBF network service. Fig. 19 b) and d) show in detail the exchange of messages between the NFVO, the SDN controller and the ARoF and OBFN agents in order to provision and remove the DL OBF connectivity service. As already mentioned, the OBFN is not integrated in the experimental scenario. In this case, we estimated the times based on measured execution times for setup and reconfiguration using the manually operated software GUI.

Fig. 20 shows the overall OBF network service delay. It is the time required by the NFVO to complete the complete lifecycle management workflow considering all the internal mechanisms, and the interaction with the resource allocation service, the BBU and RRH PNFMs, and the SDN controller for the configuration of the BBU, RRH and the OBF fronthaul. As shown, the overall delay for provisioning an OBF network service is above 134 s, the modification of the OBF network service to add or remove a beam is in the range of 65–87 s, and finally, the deletion of the OBF service is almost 18 s. It meets the 5G key performance indicators(KPI) on reducing the average service creation time cycle from 90 h to 90 min as defined by the 5G Public-Private Partnership (5G PPP) [38]. Additionally, we also provide the contribution in the overall OBF network service delay of the NFVO internal processes, resource allocation service, BBU configuration, RRH configuration, OBFN configuration, ARoF configuration, DL OBF connectivity service, and OBF UL connectivity service.

The NFVO internal processes mainly involve the time consumed in internal polling mechanisms between the components. For the provisioning and reconfiguration these are higher due to the fact that the specific parameters need to be computed and assigned, while for the removal of the beam or the removal of the OBF service the NFVO can directly proceed to the request. On the other hand, the DL/UL OBF connectivity service delay is 54 s for the instantiation of the service with one beam, 31 s for the reconfiguration of the OBF connectivity service by adding/removing beams, and just 6 s for the removal of the OBF connectivity service. This is because a cold-start of OBFN and ARoF is assumed. If the first step would be a wake-up from sleep, the times for the first step for those would be same as the reconfiguration times.

It should be noted that the time contributions of the ARoF and OBFN are measured for the current hardware control implementations and could be substantially reduced by using parallel execution of setup commands and an improved communication interface to the actual hardware microcontrollers. As an estimate, this could reduce the combined reconfiguration time of ARoF and OBFN to below 5 s.

VII. Conclusion and future work

This paper has shown the feasibility of the proposed beyond 5G fronthaul network with dynamic beamforming and -steering. We have presented the design and characterization of the developed coherent and incoherent OBFN systems, the key elements to deploy optical beamforming. On the other hand, we have fully validated the dynamic beamforming and -steering through the deployment the proposed SDN/NFV MANO architecture with dynamic OBF connectivity and network services. The measured results show that the overall delay for provisioning an OBF network service with the contribution of the different optical and radio systems (i.e., coherent and incoherent OBFNs, ARoF transceivers, BBUs with analog output/input and RRHs) is 134 s, the modification of the OBF network service to add or remove a beam is in the range of 65–87 s, and finally, the deletion of the OBF service is 18 s. It meets the 5G KPI on reducing the average service creation time cycle from 90 h to 90 min.

Future work will concentrate on the full validation of the presented OBF fronthaul system architecture with the deployment of the coherent and incoherent 4x4 OBFN systems in the testbed to perform real propagation measurements at the physical layer.

References

[1] S. Chen *et al.*, "Beam-space multiplexing: Practice, theory, and trends, from 4g td-lte, 5g, to 6g and beyond," *IEEE Wireless Communications*, vol. 27, no. 2, pp. 162–172, 2020.

[2] C. Tsokos *et al.*, "Analysis of a multibeam optical beamforming network based on blass matrix architecture," *J. Lightw. Technol.*, vol. 36, no. 16, pp. 3354–3372, 2018.

[3] D. Pliatsios, P. Sarigiannidis, S. Goudos, and G. K. Karagiannidis, "Realizing 5g vision through cloud ran: technologies, challenges, and trends," *EURASIP Journal on Wireless Communications and Networking*, vol. 2018, no. 1, pp. 1–15, 2018.

[4] R. Muñoz *et al.*, "Sdn control and monitoring of sdm/wdm and packet transport networks for 5g fronthaul/backhaul," in *2018 IEEE Photonics Society Summer Topical Meeting Series (SUM)*. IEEE, 2018, pp. 151–152.

[5] ——, "Elastic optical technologies and sdn/nfv control for 5g mobile x-haul," in *2017 IEEE Photonics Society Summer Topical Meeting Series (SUM)*. IEEE, 2017, pp. 9–10.

[6] M. Klinkowski, "Planning of 5g c-ran with optical fronthaul: A scalability analysis of an ilp model," in *2018 20th International Conference on Transparent Optical Networks (ICTON)*. IEEE, 2018, pp. 1–4.

[7] M. Masoudi, S. S. Lisi, and C. Cavdar, "Cost-effective migration toward virtualized c-ran with scalable fronthaul design," *IEEE Systems Journal*, vol. 14, no. 4, pp. 5100–5110, 2020.

[8] T. Pfeiffer, "Next generation mobile fronthaul and midhaul architectures," *Journal of Optical Communications and Networking*, vol. 7, no. 11, pp. B38–B45, 2015.

[9] N. J. Gomes and P. Assimakopoulos, "Optical fronthaul options for meeting 5g requirements," in *2018 20th International Conference on Transparent Optical Networks (ICTON)*. IEEE, 2018, pp. 1–4.

[10] I. Chih-Lin *et al.*, "Ran revolution with ngfi (xhaul) for 5g," *Journal of Lightwave Technology*, vol. 36, no. 2, pp. 541–550, 2017.

[11] N. J. Gomes *et al.*, "Boosting 5g through ethernet: How evolved fronthaul can take next-generation mobile to the next level," *IEEE vehicular technology magazine*, vol. 13, no. 1, pp. 74–84, 2018.

[12] R. Muñoz *et al.*, "SDN/NFV 5G fronthaul networks integrating analog/digital RoF, optical beamforming, power over fiber and optical SDM technologies," in *Eur. Conf. Netw. Commun. (EuCNC)*. IEEE, 2019, pp. 459–463.

[13] T. Lagkas, D. Klonidis, P. Sarigiannidis, and I. Tomkos, "5g/ngpon evolution and convergence: Developing on spatial multiplexing of optical fiber links for 5g infrastructures," *Fiber and Integrated Optics*, vol. 39, no. 1, pp. 4–23, 2020.

[14] G. Kalfas *et al.*, "Next generation fiber-wireless fronthaul for 5g mmwave networks," *IEEE Communications Magazine*, vol. 57, no. 3, pp. 138–144, 2019.

[15] S. Rommel *et al.*, "High-capacity 5g fronthaul networks based on optical space division multiplexing," *IEEE Transactions on Broadcasting*, vol. 65, no. 2, pp. 434–443, 2019.

[16] R. Muñoz *et al.*, "Bluespace's sdn/nfv architecture for 5g sdm/wdm-enabled fronthaul with edge computing," in *2018 European Conference on Networks and Communications (EuCNC)*. IEEE, 2018, pp. 403–9.

[17] C. Mitsolidou *et al.*, "A 5G C-RAN optical fronthaul architecture for hotspot areas using OFDM-based analog IFoF waveforms," *Appl. Sci.*, vol. 9, no. 19, p. 4059, Sep. 2019.

[18] S. Rommel *et al.*, "Towards a scaleable 5G fronthaul: Analog radio-over-fiber and space division multiplexing," *J. Lightw. Technol.*, vol. 38, no. 19, pp. 5412–5422, 2020.

[19] M. Morant *et al.*, "Experimental demonstration of mm-wave 5g nr photonic beamforming based on orrs and multicore fiber," *IEEE Transactions on Microwave Theory and Techniques*, vol. 67, no. 7, pp. 2928–2935, 2019.

[20] R. Muñoz *et al.*, "Sdn/nfv control and orchestration of dynamic optical beamforming services for beyond 5g fronthaul networks," in *Eur. Conf. on Optical Communication (ECOC)*. IEEE, 2020.

[21] A. Mukherjee, B. Rojas, and H. Ujhazy, "Business models for the long-term storage of internet of things use case data," IDC report, 2020.

[22] F. Giust, X. Costa-Perez, and A. Reznik, "Multi-access edge computing: An overview of etsi mec isg," *IEEE 5G Tech Focus*, vol. 1, no. 4, p. 4, 2017.

[23] blueSPACE, "D2.2 – physical architecture, system and network requirements," https://www.bluespace-5gppp.eu/s/D22-D8-Physical-architecture-system-and-network-requirements.pdf.

[24] A. Meijerink *et al.*, "Novel ring resonator-based integrated photonic beamformer for broadband phased array receive antennas—Part I: Design and performance analysis," *J. Lightw. Technol.*, vol. 28, no. 1, pp. 3–18, Jan. 2010.

[25] C. Roeloffzen *et al.*, "Enhanced coverage though optical beamforming in fiber wireless networks," in *Intl. Conf. Transpar. Opt. Netw. (ICTON)*, Jul. 2017, paper TH.A2.1.

[26] C. Zhu *et al.*, "Silicon integrated microwave photonic beamformer," *Optica*, vol. 7, no. 9, pp. 1162–1170, Sep 2020.

[27] G. Serafino *et al.*, "A photonic beamforming network based on phase shifters for microwave wide-band applications," in *2019 21st International Conference on Transparent Optical Networks (ICTON)*, 2019.

[28] A. B. Smolders *et al.*, "Building 5g millimeter-wave wireless infrastructure: Wide-scan focal-plane arrays with broadband optical beamforming," *IEEE Antennas and Propagation Magazine*, vol. 61, no. 2, pp. 53–62, 2019.

[29] D. Konstantinou *et al.*, "5g ran architecture based on analog radio-over-fiber fronthaul over udwdm-pon and phased array fed reflector antennas," *Optics Communications*, vol. 454, p. 124464, 2020.

[30] M. Xiao *et al.*, "Millimeter wave communications for future mobile networks," *IEEE J. Sel. Area Commun.*, vol. 35, no. 9, pp. 1909–1935, Sep. 2017.

[31] F. Azendorf *et al.*, "Characterization of multi-core fiber group delay with correlation otdr and modulation phase shift methods," in *Opt. Fiber Commun. Conf. (OFC)*, 2020, paper M2C.5.

[32] J. Brenes *et al.*, "Network slicing architecture for sdm and analog-radio-over-fiber-based 5g fronthaul networks," *Journal of Optical Communications and Networking*, vol. 12, no. 4, pp. B33–B43, 2020.

[33] C. Manso *et al.*, "Tapi-enabled sdn control for partially disaggregated multi-domain (ols) and multi-layer (wdm over sdm) optical networks," *Journal of Optical Communications and Networking*, vol. 13, no. 1, pp. A21–A33, 2021.

[34] 3GPP TS 38.104, "NR: Base station (BS) radio transmission and reception," Sep. 2019, 3GPP Rel. 15, V15.7.0.

[35] "ONF transport API (TAPI) github," https://github.com/OpenNetworkingFoundation/TAPI, accessed: 2020-06-23.

[36] "TAPI OBFN extensions," https://github.com/CTTC-ONS/bluespace/tree/master/TAPIext, accessed: 2020-07-20.

[37] S. Rommel *et al.*, "Real-time high-bandwidth mm-wave 5g nr signal transmission with analog radio-over-fiber fronthaul over multi-core fiber," *EURASIP J. Wireless Commun. Netw.*, 2021.

[38] To-Euro-5G, "D4.4 final report on 5G PPP KPI progression," 2019. [Online]. Available: https://ec.europa.eu/research/participants/documents/downloadPublic?documentIds=080166e5c63e0d96&appId=PPGMS

Dr. Raul Muñoz (IEEE SM'12) is graduated in Telecommunications Engineering and received a Ph.D. degree, both from the Universitat Politècnica de Catalunya (UPC), Spain. He is Head of the Optical Networks and Systems Department at CTTC. He has participated or promoted over 50 R&D projects funded by EC, Spanish Research programmes, and industrial contracts. He has been Project Coordinator of the FP7 EU-Japan STRAUSS project, and the H2020-MSCA-ITN ONFIRE project. He has served as general chair of ONDM 2020 & WWRF39, and TPC chair of ECOC 2015 & ONDM2019. He was elected academic member of the 5G IA Board, the Steering Board of WWRF and the Networld2020 ETP (2015-2017). He has published over 85 JCR journal papers, 275 international conference papers, and 3 patents.

Dr. Simon Rommel (S'15 M'18) obtained his B.Sc. from University of Stuttgart, Germany in 2011 and in 2014 obtained M.Sc. degrees in Photonic Networks Engineering from Aston University, Birmingham, UK and Scuola Superiore Sant'Anna, Pisa, Italy. He completed his Ph.D. in 2017 at Technical University of Denmark, Kongens Lyngby, Denmark with research focused on photonic-wireless convergence and millimeter-wave radio-over-fiber, including a research stay at the National Institute of Information and Communications Technology, Koganei, Tokyo, Japan. Since 2017 he is with Eindhoven University of Technology, currently as assistant professor, continuing his work photonic and radio frequency technologies with a strong focus on implementations for 5G. He contributed to multiple national and European research projects, incl. H2020 blueSPACE as technical manager. Dr. Rommel is a member of IEEE, OSA, IET and VDE.

Dr. Paul van Dijk MBM [M] (Vice President Strategy and Innovation) received his MSc. (1992) and Ph.D. (1997) in Applied Physics from the Technical University Eindhoven in the field of materials science and materials characterization using high energy ion beam analysis techniques. Paul holds a Master of Business Marketing from TIAS Nimbas School (2002). He started in 1997 at High Voltage Engineering Europe, followed by 11 years at ASML product marketing for Special Applications. As co-founder of SATRAX (2010), Paul acted as CEO and was responsible for Supply chain management, Business development and marketing of the integrated microwave photonics products.

Juan Brenes [M], received his degree in Telematics Engineering at the Universidad de Montevideo, Uruguay, in 2011 and his Master's degree in Telematics at the Universidad Carlos III de Madrid (UC3M), Madrid, Spain in 2015. At UC3M his research focus was on BGP, Data Centre architectures and video streaming applications. For the last four years he has been working as a researcher and consultant in the areas of NFV, SDN and 5G technologies for different companies and participating in several EU funded projects (METRICS, 5G-TRANSFORMER, TRILOGY II, etc). He currently works at Nextworks as Senior R&D Systems and Software Engineer, being actively involved in 5G research projects (blueSPACE, 5G EVE, 5Growth, 5GZORRO).

Evangelos Grivas Evangelos Grivas received his BSc in Physics from Aristotle University of Thessaloniki, Greece in 2002, and his MSc in Microelectronics from University of Athens, Greece in 2004. He was with the Institute of Microelectronics, NCSR "Demokritos", from 2004 to 2006. He was with the Optical Communications Laboratory, University of Athens, Greece, from 2005 to 2012, working for his PhD on Optical Communications, where he also served as research associate on contract, leading the design and development of numerous demonstrators. He served as the head of R&D in Eulambia Advanced Technologies from 2013 to 2020. His current research interests include ARoF for 5G communications. He is currently with NanoMEGAS SPRL.

Carlos Manso received his B.S. and M.S. degrees in Telecommunications Engineering from Universitat Politècnica de Catalunya (UPC) in Barcelona (Spain) in 2016 and 2018, respectively. He has been working in CTTC as a research assistant since 2018. Since 2020 he is also a PhD candidate on SDN networks, focusing on cloud native transport networks orchestration and machine learning for SDN networks.

Dr. Chris Roeloffzen [M] (Group Leader / Chief Scientific Officer) received his MSc degree in physics from the University of Twente (1998) and his Ph.D. degree in electrical engineering (2002). He became assistant professor in the Telecommunication Engineering Group, University Twente, where he was involved with research and education on integrated microwave photonic systems. He founded of the company SATRAX (2009) as Chief Technology Officer. He is the Technical Program Committee co-chair of IEEE Topical Meeting of Microwave Photonics, MC member of the EU COST 16220: European Network for High Performance Integrated Microwave Photonics and member of the Management Team.

Dr. Ricard Vilalta (Girona, 1983) graduated in telecommunications engineering in 2007 and received a Ph.D. degree in telecommunications in 2013, both from the Universitat Politècnica de Catalunya (UPC). He joined CTTC in 2010, and he is a senior researcher in the Optical Networks and Systems Department. He is an active contributor in several standardization bodies such as ONF (OTCC), ETSI (NFV, ZSM), and IETF (CCAMP, TEAS). He is leading open source contributions and features in ETSI Open Source MANO (OSM). He has been involved in several international, EU, national and industrial research projects.Currently, he is Project Coordinator of 5GPPP TeraFlow project.

Dr. Josep M. Fàbrega received his PhD degree in signal theory and communications from UPC-BarcelonaTech, Barcelona, Spain, in 2010. Currently he is a senior researcher in the Optical Networks and Systems Department of CTTC, Castelldefels, Spain. He has participated in over 21 R&D projects either funded by industry or the EU and Spanish national Research programmes. He is the author of more than 170 papers. His research interests include broadband optical communications emphasizing on advanced modulation formats and optical signal delivery over novel network architectures. Dr. Fabrega is IEEE Senior Member since 2017.

Giada Landi [F] received the degree in Telecommunication Engineering at the University of Pisa, Italy, in 2005. Currently she is project manager at Nextworks, where she is the leader of the R&D architectures design activities. Her main research areas include SDN, NFV, MEC, cloud computing, orchestration and cloud-to-network interactions. Some of her past research activities focused on ASON/GMPLS and PCE architectures, control plane for wireless access networks and inter-technology mobility. She has participated in several national and EU FP7 and H2020 projects, as well as in industrial projects on PCE, SDN and NFV topics. She is currently active in the H2020 5G-EVE, 5G-CroCo, 5GROWTH, blueSPACE and QAMeleon projects and she is contributing in ETSI MEC as member of the special task force on MEC Testing Framework.

Dr. Ramon Casellas (SM'12) graduated in 1999 from UPC, Barcelona and from the ENST, Paris, where he completed a PhD degree in 2002. In 2006, he joined the CTTC, currently holding a Senior Researcher position. His research interests include Optical Networks, GMPLS/PCE, SDN and NFV, having participated in several R&D projects. He has co-authored 5 book chapters, over 200 journal and conference papers and 5 IETF RFCs. He has been TPC member of conferences such as ECOC, OFC, ONDM or ICC and he is a regular reviewer for IEEE CommMag, IEEE Network, IEEE/OSA JLT and IEEE JOCN (currently serving as a Guest Editor).

Dr. Ricardo Martínez (SM'14) received the M.Sc. and Ph.D. degrees, both in telecommunications engineering, from the UPC–BarcelonaTech University, Barcelona, Spain, in 2002 and 2007, respectively. He has been actively involved in several EU public-funded and industrial technology transfer projects. Since2013, he is a Senior Researcher at CTTC in Castelldefels, Spain. His research interests include control and orchestration architectures for heterogeneous and integrated network, and cloud infrastructures along with advanced mechanisms for provisioning/recovering quality-enabled services.

Prof. Idelfonso Tafur Monroy is Professor in Photonic Terahertz Systems at the department of Electrical Engineering of Eindhoven University of Technology since 2017 and since 2018 director of the Photonic Integration Technology Center (PITC). His research interests are in the area photonics technologies for Terahertz systems, converged electronic-photonic integrated circuits for applications in secure communications, sensing and computing. He is co-author of over 500 journal and conference papers and has graduated 22 PhD students. He is co-founder of the start-up Bifrost Communications on optical fiber access solutions.